Regional Studies in Marine Science 40 (2020) 101475

Contents lists available at ScienceDirect

Regional Studies in Marine Science

journal homepage: www.elsevier.com/locate/rsma

A step towards high resolution modeling of the central Faroe shelf circulation by FarCoast800

Sissal V. Erenbjerg [a,c,*], Jon Albretsen [d], Knud Simonsen [a,b], Anne D. Sandvik [d], Eigil Kaas [c]

[a] Fiskaaling - Aquaculture Research Station of the Faroes, við Áir 11, FO-430 Hvalvík, Faroe Islands
[b] University of the Faroe Islands, J. C. Svabosgøta 14, FO-100 Tórshavn, Faroe Islands
[c] Niels Bohr Institute, Copenhagen University, Juliane Maries Vei 30, DK-2100 Copenhagen, Denmark
[d] Institute of Marine Research, P.O. box 1870 Nordnes, NO-5817, Bergen, Norway

ARTICLE INFO

Article history:
Received 31 January 2020
Received in revised form 1 September 2020
Accepted 17 September 2020
Available online 9 October 2020

Keywords:
North Atlantic
Faroe shelf
Circulation
Numerical modeling
Aquaculture

ABSTRACT

This paper describes the FarCoast800 model setup for the Faroe shelf and the validation towards observations. We found that the circulation was in accordance with observations on the shelf and the upper ∼500m of the water column, away from the lateral boundaries. Furthermore, we found high correlations between the model and observations for the on-shelf water, in particular for short-term variations of temperature, demonstrating the importance of high resolution atmospheric forcing. A main challenge for this study was the lateral boundary conditions at all four open boundaries in the varying and steep bathymetry of the FarCoast800 model setup. We also investigated the origin of water reaching the different areas of the shelf. Notably our results indicated intrusion of water originating from the East Icelandic Current into the deeper areas on the eastern part of the Faroe shelf.

Our long term motivation of the study was to investigate the capability of the model to drive an even higher resolution ROMS model setup for the central Faroe shelf, enabling the resolution of processes on a 100m scale or less. The study concludes that FarCoast800 can drive a high-resolution nested model area on the Faroe shelf.

Here we present a Regional Ocean Model System (ROMS) model setup for the Faroe shelf with a horizontal resolution of 800m x 800m and 35 vertical layers. The model setup is forced by a high resolution atmospheric model, and forced by a 4km x 4km horizontal resolution version of the ROMS model on the lateral boundaries. We name our model setup FarCoast800. The model setup was run for the entire sample year 2013.

1. Introduction

The Faroe Islands is an archipelago located in the Northeast Atlantic Ocean (Fig. 1). The greatest contribution to the economy is from the ocean, through the off-shore fishery and the fish farms located in the fjords and straits (Dam, 2019). This increases the interest towards understanding the circulation on the shelf in relation to both ecology on the shelf, and dispersion between the fish farming sites. The long term strategic goal of our work has been to assist studies on matters regarding fish farming through providing helpful scientific knowledge for the industry of fish farming.

The central location of the Faroe Islands on the Greenland–Scotland Ridge (Fig. 1 and Section 2), ensures that the area is included in a large number of numerical circulation models on the ocean exchange between the Atlantic Ocean and the Arctic Ocean. Nonetheless the efforts to investigate the water properties and circulation more locally on the Faroe shelf by the means of numerical models are still limited, with only two prior model setups. The first model study by Rasmussen et al. (2014) uses a modified version of the 3D HYbrid Coordinate Ocean Model (HYCOM) (Chassignet et al., 2007), with a horizontal resolution ranging from 750–1300 m in a hindcast run for the years from 2000 to 2009. The study of Rasmussen et al. (2014) quantifies the exchange of the shelf water mass, and explains the processes controlling the variability between years of the Faroe shelf spring bloom. The second model study by Kragesteen et al. (2018) and Patursson et al. (2017) uses results from a 2D numerical tidal model with a spatial resolution of 100 m, to identify the significant contribution of the tidal currents and the residual currents generated by tidal rectification in dispersion of parasites between fish farming sites.

For the atmosphere in windy and mountainous areas like the Faroe Islands, the large scale wind flow is highly modified by the local topography. The wind forcing on the upper

* Corresponding author at: Fiskaaling - Aquaculture Research Station of the Faroes, við Áir, FO-430 Hvalvík, Faroe Islands.
E-mail address: sissal@fiskaaling.fo (S.V. Erenbjerg).

https://doi.org/10.1016/j.rsma.2020.101475

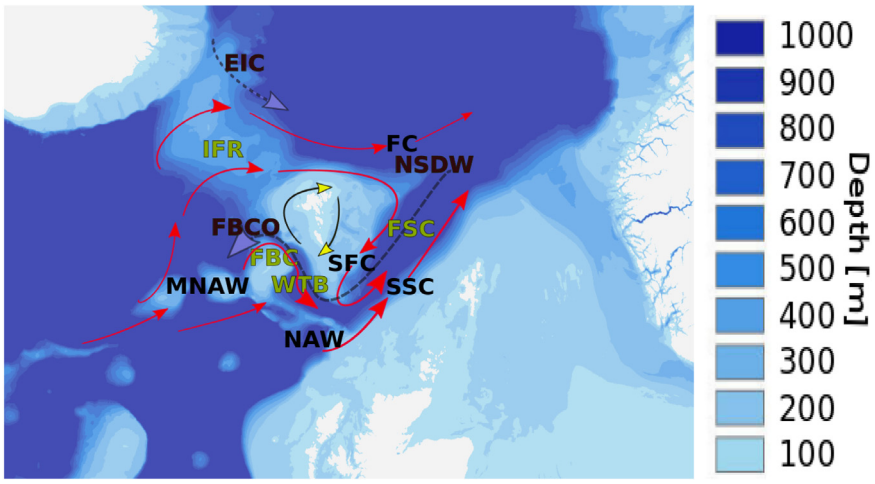

Fig. 1. Bathymetry of the area and schematic arrows of the main flow pathways. Continuous arrows indicate flow of Modified North Atlantic Water (MNAW) and North Atlantic Water (NAW) in the upper layers (red), the cold Norwegian Seas Deep Water (NSDW) (purple), the colder and fresh East Icelandic Current (EIC) (purple) and the clockwise residual current on the shelf (yellow). The other abbreviations are the Faroe Bank Channel (FBC), the Faroe Bank Channel Overflow (FBCO), the Wyville Thomsen Basin (WTB), the Faroe Shetland Channel (FSC), the Iceland Faroe Ridge (IFR), Faroe Current (FC), South Faroe Current (SFC) and Scottish Slope Current (SSC). Redrawn from Larsen et al. (2009) and Hansen et al. (2017). Map is by courtesy of Anders Nygård (ArcGIS). (For interpretation of the references to color in this figure legend, the reader is referred to the web version of this article.)

ocean has a large spatial and temporal variability. High resolution atmospheric forcing is important for distributing the precipitation correctly in mountainous areas (lee and lo side of mountains), and inclusion of high quality atmospheric forcing will increase the ability to simulate the ocean circulation in a realistic way (Myksvoll et al., 2012; Skogseth et al., 2007).

To represent the circulation in a complex bathymetry a 3D dynamical ocean model is imperative. However, Forcing a high-resolution coastal model from all geographical directions demands good precision on the offshore model, as biases will propagate towards the coast. One ocean model that has been proven effective for regions with many fjords and highly varying and steep bathymetry, such as our model domain (Section 2), is the Regional Ocean Model System (ROMS) (Shchepetkin and McWilliams, 2005), such as it is applied for the Norwegian coast in the NorKyst800 model setup (Lien et al., 2013).

Here we adapt the NorKyst800 model setup, see e.g. applications in Huserbråten et al. (2018) and Myksvoll et al. (2018) with 800 m × 800 m resolution and 35 vertical layers to the Faroe shelf, aiming at providing further insight into the general circulation on the Faroe shelf and providing validated boundary conditions for future higher resolution simulations of the central shelf and coastal regions.

A summary of present knowledge of the relatively complex circulation in the region is provided in Section 2. The model setup, applied forcing and simulation is described in Section 3.1, and observed data sets for validation are presented in Section 3.4. The model output and validation towards observations are provided in Section 4, which is followed by a discussion in Section 5 and concluding remarks in Section 6.

2. Hydrographic area description

The ocean surrounding the Faroe Islands (Fig. 1) is for the off-shelf waters, in the upper layers dominated by water of Atlantic origin (Larsen et al., 2008, 2009; Hansen and Østerhus, 2007; Hansen et al., 2017). The water entering the area from the west is traditionally termed Modified North Atlantic Water (MNAW), while to the south over the Scottish slope the warmer and more saline North Atlantic Water (NAW) is carried by the Scottish Slope Current (SSC) (Hansen et al., 2017). In the open northwest Atlantic the MNAW splits into two branches. One branch flows over the banks to the southwest towards the Faroe Shetland Channel (FSC), where it joins the SSC. The other branch is flowing north of the Faroe Islands, after crossing the Iceland Faroe Ridge (IFR) between the Faroe Islands and Iceland, it becomes focused into the narrow Faroe Current (FC) north of the Faroe Islands (Hansen et al., 2017). On the eastern slope of the Faroe Bank (FB) there is a southward flowing branch of MNAW, which either joins the MNAW water in the Wyville Thomson Basin (WTB) (Fig. 1), or is recirculated in the Faroe Bank Channel (FBC) and flows northward again along the western Faroe shelf (Hansen et al., 2017).

Northeast of the Faroe Islands the MNAW continues northeastward into the Norwegian Sea, but a branch turns southward along the eastern flank of the Faroe shelf and is retroflected eastward in the FSC. This southwestward flow along the eastern slope of the Faroe shelf is named the Southern Faroe Current (SFC) by Hátún (2004). The strength of these two branches may vary (Hátún et al., 2005).

To the north the fresher and colder water of Arctic origin is transported towards the area east of IFR by the East Icelandic Current (EIC) (Beaird et al., 2016). Approaching the Faroe shelf, this water is overlaid by the warmer and more saline water of Atlantic origin, but is leaning towards the shelf slope to the north and is flowing southwards along the slope of the eastern shelf (Hansen et al., 2010). Along its path it is diluted by the surrounding water, and it is generally considered to reflect eastward in the FSC, although traces of this water are also seen as an intermediate layer in the out-flowing water in the FBC (Hansen and Østerhus, 2000; Ullgren et al., 2014). The appearance of the EIC water explains the generally slightly colder and fresher water east of the Faroes compared to the western side (Hansen et al., 2017; Hátún, 2004). However, occasional mixing onto Faroe shelf is seen from the more saline and warmer SSC (Larsen et al., 2008).

The deeper layers are dominated by the relatively cold and fresh Norwegian Sea Deep Water (NSDW), which fills up the deeper part of the Norwegian Sea Basin to the east of the Faroe Islands. This modified NSDW flows through FSC to the south and continuous through WTB to the FBC as the Faroe Bank Channel Overflow (FBCO) west of the Faroe shelf, contributing to the North Atlantic Deep Water (NADW) formation (Hansen et al., 2016, 2017).

The on-shelf waters consist of a mixture of the surrounding waters (Larsen et al., 2008) and is characterized by relatively

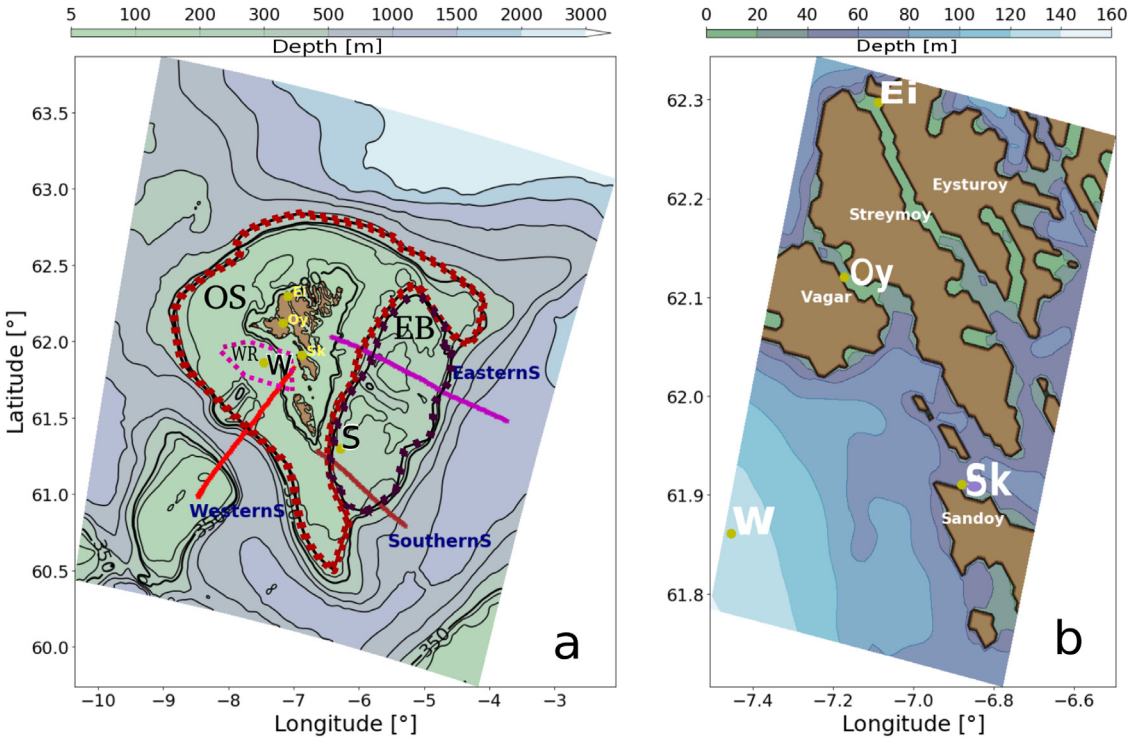

Fig. 2. **a**: The Faroe shelf and the model domain. The black thin lines shows the bottom contours for 50 m, 100 m, 300 m, 500 m, 700 m, 1000 m, 1500 m, 2000 m, 3000 m. (1) The thick red line WesternS indicates the positions of the hydrographic section from the Faroe Shelf at 61.8°N 7.0°W westwards through the FBC out to the FB at 61.0°N 8.5°W. The thick purple line EasternS indicates the positions of the hydrographic section from the Faroe shelf at 62.0°N 6.4°W eastwards of the Faroe shelf into the FSC to the east at 61.5°N 3.7°W . (2) The stations (see text) by letters W and S are locations of timeseries on the OS depth greater 100 m. The stations (see text) Ei, Oy and Sk are locations of coastal timeseries depth less than 100 m. (3) The three areas OS (red broken line), WR (pink broken line) and EB (purple broken line) are largely redrawn from Eliasen et al. (2017b). **b**: Zoom on the locations of the coastal stations Ei, Oy and Sk as well as the bathymetry. (For interpretation of the references to color in this figure legend, the reader is referred to the web version of this article.)

strong tidal currents with clockwise residual currents around the islands (Larsen et al., 2008; Kragesteen et al., 2018). Moreover the on-shelf waters are divided into three domains based on ocean dynamics (Eliasen et al., 2019; Larsen et al., 2008, 2009) and phytoplankton variability (Fig. 2) (Eliasen et al., 2017a, 2019). The Central Shelf (CS) is separated from the rest of the water on the shelf by a tidal front at the ∼100–150 m depth contour named the Faroe Shelf Front (FSF) and is permanently well mixed due to the relatively strong tidal currents (Larsen et al., 2009). Studies of the abundance and timing of blooming of phytoplankton (Eliasen et al., 2017a, 2019) shows that CS has different characteristics than the remaining shelf, which may be divided into two additional separate areas. One area covering the banks on the eastern shelf, the Eastern Banks (EB) (Fig. 2) and the remaining Outer Shelf (OS). The highest averages and variances in chlorophyll concentrations are found in a region on the western side of the shelf, termed Western Region (WR), and the entire OS varies similar to WR (Eliasen et al., 2017a). The different phytoplankton phenology in these three distinct areas on the shelf is also reflected in the variability of zooplankton (Jacobsen et al., 2018).

From the influence of the relatively warm MNAW, which embeds the Faroe shelf, the atmosphere cools the ocean the entire year except for the high summer months. This cooling is most effective in the shallower and permanently mixed CS, and is reflected in a ∼1 °C lower temperature (Larsen et al., 2009). Also, the CS has ∼0.1 psu fresher water than in OS, which is explained to be due to enhanced precipitation because of orographical effects on the islands (Larsen et al., 2009). The residence time is 1–2 months, but is likely highly variable (Larsen et al., 2009; Rasmussen et al., 2014; Eliasen et al., 2016). The separation of the on-shelf waters and the surrounding open ocean waters, as well as the separation of the on-shelf water into the CS and OS are crucial for the ecology in the area and significant in the recruitment of several commercial important fish stocks (Larsen et al., 2008; Eliasen et al., 2017a, 2019; Jacobsen et al., 2018). This separation plays a significant role in maintaining drift particles, including sea lice, within the CS and a better understanding of the circulation on the shelf is crucial in developing models and strategies for management of the local aquaculture industry (Kragesteen et al., 2018).

3. Material and methods

3.1. The FarCoast800 model

The ROMS model setup applying 800 m × 800 m horizontal resolution around the Faroe shelf, hereafter named FarCoast800, was originally adapted from the Norwegian Coastal model, NorKyst800 applying the same resolution. Such coastal model systems are developed as a compromise between geographical extension of the model domain and sufficient grid resolution to provide realistic hydrodynamic information of coastal zones. Our version covers the entire Faroe Shelf and the Faroe Bank to the west of the Faroes and extends into the deep water surrounding the area to the east, north and west, and the Scottish shelf to the south (Fig. 2a). Our main interests are the shallower regions, above the 350 meter contour line in Fig. 2a. FarCoast800 is implemented using ROMS as the hydrodynamic model (e.g. Shchepetkin and McWilliams (2005) and Haidvogel et al. (2008) , or see http://myroms.org). ROMS is a state-of-the-art, three-dimensional, free-surface, primitive equation numerical ocean model using a generalized terrain-following s-coordinate in

the vertical. The FarCoast800 model applies 35 vertical levels and was set up with enhanced resolution in the upper ~50 m.

The Chapman boundary condition (Chapman, 1985) was used for the free-surface boundary condition and the lateral boundary condition by Flather (1976)) was applied for the barotropic velocity. As described by Marchesiello et al. (2001) and as applied in our model set-up, ROMS has an option for providing radiation conditions on outflow and nudging to a known exterior value on inflow for 3D momentum and tracers. This is here implemented as a variation on the radiation condition, requiring two timescales, namely the inflow nudging timescale and the outflow nudging timescale. Here, the nudging on inflow was 120 times larger than on the outflow. For vertical turbulence, the local closure scheme was based on the Generic Length Scale (GLS) parameterization (Umlauf and Burchard, 2003).

Lateral boundary conditions and initial fields conditions are retrieved from the Nordic Seas 4 km numerical ocean model hindcast archive (SVIM), which covers the area from the North Atlantic west of Ireland, the Nordic Seas and into the Arctic to the north and is described in Lien et al. (2013). Note that the boundaries in the SVIM-model after 2009 applied monthly climatological values of currents and hydrography, as the provider, the Simple Ocean Data Assimilation set (SODA; Carton et al., 2000; Carton and Giese, 2008) was released with a final simulation date in 2009 (version 3.6.1). The years of SODA fields aggregated to force the SVIM model are 2000–08. This implies that the open boundaries in the FarCoast800 simulation applied monthly climatological external forcing as input and then mainly resolved the seasonal variability only. The tidal forcing was applied along the open boundaries and interpolated from the global TPXO7.2 (Egbert and Erofeeva, 2002).

The simulation was initialized January 1st, 2013 from SVIM 4 km state and was run for one year until December 31st, 2013. The first 1–2 months should then be considered as a spin-up period.

3.2. Atmospheric forcing, WRF

The atmospheric forcing is obtained from simulations with the Weather Research and Forecasting (WRF) model (WRF, http://www.wrf-model.org/) The model was configured with horizontal grid resolutions of 9-3-1 km, where the 1 km resolution domain covered the area of interest and was used as forcing for the ocean model. See Myksvoll et al. (2012) for more details on the configuration.

3.3. Fresh water forcing, rivers

River runoff is neglected except for the runoff into the strait between two largest islands, Streymoy and Eysturoy (Fig. 2 right), where the river runoff is estimated from various freshwater gauges (courtesy to the local energy producer, SEV) and the orographic model by Davidsen et al. (1994).

3.4. Observed data

3.4.1. Hydrographic sections

The Faroe Marine Research Institute (FAMRI) runs a monitoring program, which includes regular hydrographic surveys 2–4 times per year along standard sections radiating from the islands and into the deep waters east, north, west and south of the Faroe shelf. Here we compare with the western section (Fig. 2a) which intersects the FBC and FB to the west and has hydrographic data available from cruises in February, May and August/September 2013. We also compare with the section across the eastern shelf from cruises in February and May 2013, and, since the eastern section was not done on the August/September cruise, we compare to the southern section in August/September 2013.

3.4.2. Temperature and salinity time series

The location of the three coastal stations are shown in Fig. 2a and b as Ei, Oy and Sk. Temperature is acquired at all stations, while salinity is only available at station Sk.

At station Sk water is pumped from 18 m depth in a tidally well mixed strait. Salinity samples are taken every 4–7 day (since 1997) by FAMRI (www.hav.fo) (Larsen et al., 2008). Temperature at station Sk is measured every 5 min. FAMRI have operated the tidal-gauge station Oy every 30 min since 1991 (Larsen et al., 2008). The remaining coastal station Ei is a tidal-gauge station located in the harbor and operated by the Office for Public Works (OPW) (www.landsverk.fo).

Stations W and S (Fig. 2a) are temperature loggers mounted close to the bottom and at 5 m depth, operated by FAMRI, on the moorings on semi-permanent wave-riders operated by OPW (Eliasen et al., 2017a).

4. Results and comparison with observations

In this section the model results are described and compared with observations. Our main interest is the circulation on the shelf, however, the off-shelf circulation is important for the on-shelf circulation. Thus the model performance for the water surrounding the shelf, is described prior to the model results for the outer and inner shelf respectively. Due to the limitation of observations and our sample year only running through 2013, we also included results from February, with care, despite this is considered part of the spin-up period.

4.1. Ocean currents in FarCoast800

The annual barotropic flow is shown in Fig. 3. Here, as expected from the literature and presented in Fig. 1: The MNAW bifurcates prior to the FB. One branch travels northward and continues along the northern edge of the Faroe shelf as part of the FC. North–northeast of the Faroe shelf at 63°N and 5°W the FC bifurcates and a well defined flow follows the bathymetry southwards in agreement with the velocity estimates obtained for the upper 100 m from a ferry mounted acoustic Doppler current profiler (ADCP) by Rossby and Flagg (2012). Entering the FSC the majority of this flow is recirculated into the SSC, as suggested by Hansen et al. (2017, e.g). However, the innermost fraction of the flow is crossing the southern tip of the shelf and continues northward along the shelf edge on the western side of the islands. The SSC is evident in the southern part of the model domain in congruence with Rossby and Flagg (2012). From the square at 60°N-61°N and 5°W-7°W, it appears that the SSC is partly fed by NAW from the boundary conditions to the south, but also with the other, southward traveling, branch of the MNAW bifurcating prior to the FB. The southward traveling branch along the FB, is strongly dominated by high velocities in the upper layers (Figs. 4d and S2). This is not in accordance with Hansen and Østerhus (2007). The main contribution to the mean annual barotropic flow is from the upper layers (Figure S2). The bottom layers have EIC water along the IFR from the north and the NSDW from the northeast (Figs. 8, 9 and S3) as expected from Fig. 1.

The spurious boundary currents to the north and northeast of the model domain are not appearing in the 4 km × 4 km model forcing (Figure S1), suggesting this to be a boundary condition artifact in the current model set-up.

4.2. Off-shelf water properties

Seasonal means of temperature, salinity, density and velocity along the hydrographic standard sections west and east of the shelf (WesternS and EasternS in Fig. 2a) are extracted from the model simulations following the validation approach by Rasmussen et al. (2014).

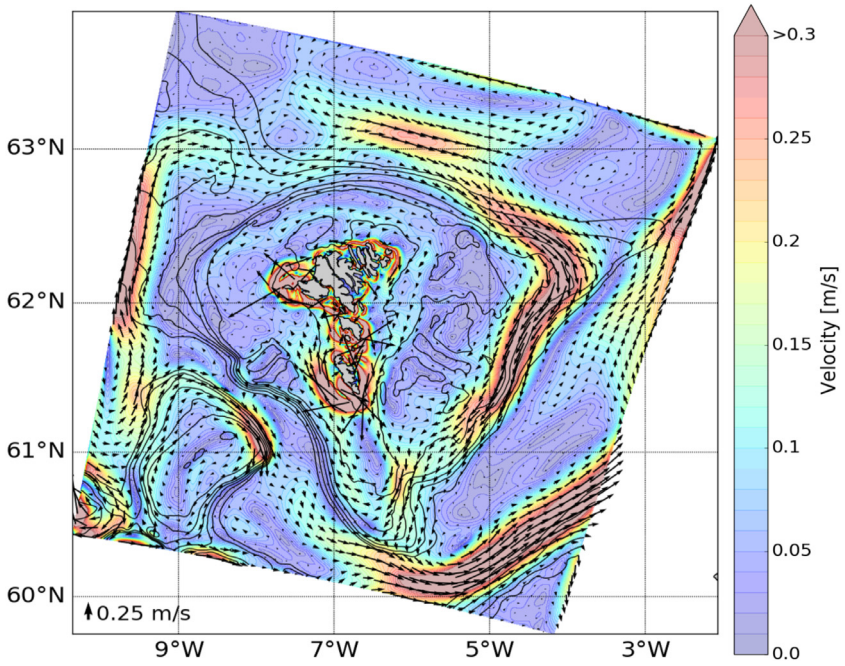

Fig. 3. Modeled annual mean barotropic flow. The colors indicate the speed (m/s), the velocity is given by the arrows. The speed is the length of the arrows.

4.2.1. Off the western shelf

The WesternS section (Fig. 2a) begins near land off the coast of the island Sandoy (Fig. 2b), and traverses the western shelf, the FBC and ends on the FB. This section is ∼120 km long and the deepest point in the section is 870 m deep around 8°W (Fig. 4).

Seasonal average temperature from June, July and August (JJA) is shown in Fig. 4a. The temperature gradients, down to ∼600 m, are tilting towards the shelf, as expected from geostrophy (Margules equation), during all seasons (Figure S4). Around 600–700 m depth the temperature isotherms are flattening and the water colder than one degree has a horizontal contour line. This is in accordance with Hansen and Østerhus (2007) and Hansen et al. (2017). Furthermore, we identify the water warmer than 7 °C depicted in Fig. 4a to be MNAW as do Hansen and Østerhus (2007).

The annual modeled mean temperature in the bottom layer in the FBC is 0.3 °C. This is warmer than the running 3-year average bottom temperature for the year 2013 of about -0.35 °C in the almost continues recordings from 1995–2015 by Hansen et al. (2016). Over the span of the record there is an increase in the bottom temperature of the order of 0.1 °C (Hansen et al., 2016). The model temperature variation in the deepest part of the FBC has a bias of up to 0.8 °C compared to what was seen in the observations for the year 2013 (Hansen et al., 2016).

Salinity in JJA at SectionW (Fig. 4b) has the same trend as the temperature in the intermediate part of the water column. Here, again the gradient lines are tilting towards the Faroe shelf. The MNAW is the more saline water (35.15<) and the NSDW is the less saline (35.0>) water in the deeper part of FBC in accordance with Hansen and Østerhus (2007) and Hansen et al. (2016, 2017). When comparing daily mean with the cruise data (Figs. 7 and 9) it is clear that the salinity levels are slightly underestimated, but the main structures are still captured for the westernS all plots.

Density is shown in Fig. 4c. The density generally follows the temperature structure from Fig. 4a in the upper part and both the salinity and temperature structure in the lower part. Again the isolines are tilting towards the Faroe shelf. The density is calculated from temperature and salinity and is thus affected by the biases in both temperature and salinity.

The northward velocity component, is shown in Fig. 4d for JJA, and the FBCO is recognized as the northward current in the model simulation below 600 m depth. Maximum values of the FBCO are along the flank of FB, decreasing towards the Faroe shelf, as expected from potential vorticity conservation (Hansen and Østerhus, 2007). There is a weak seasonal variation in the overflow, which in our model is weakest during JJA and strongest in MAM (Figure S9), which is out of phase with the observations showing maximum current in August and minimum in February (Hansen et al., 2016). We also see a short period during July in the model simulation were the FBCO is going in the opposite direction, contributing to the low average northward velocity during JJA (∼0.1 m/s). This is likely a constrain from boundary conditions (Figure not shown).

Along the upper eastern flank of the FB, a divaricate of the MNAW persist as a strong southward flow (Fig. 4d) during all seasons. In the model simulation this flow has a seasonal variation and is strongest in the summer months (Figure S9). This branch mainly contributes to the SSC, yet a small fraction of the easternmost water mass seems to be recirculated and continues northward along the western Faroe shelf (Fig. 4d at −7.8°W and Fig. 3).

4.2.2. Off the eastern shelf

The section EasternS (Fig. 2a) is across the eastern shelf. It begins near the island Eysturoy (Fig. 2b) and traverses the EB, continuing into the mid FSC. The maximum depth is 1245 m (Fig. 5).

In the FSC the deep water (>800 m) is dominated by NSDW with temperatures below 0.0 °C, and salinity less than 34.94 (Fig. 5a,b); with minimum seasonal temperature average in the bottom layer of approximately -0.4 °C during all seasons. This is in agreement with observations (Hansen et al., 2017). The current in the deepest part is southward on the Faroe side, and becomes weaker in the central FSC (Fig. 5d). The density isolines follow both the salinity isolines and the temperature isolines in the FSC Fig. 5a,b, and c.

In the intermediate water depth at about 500–800 m, there is a weak salinity minimum during all seasons, with values below

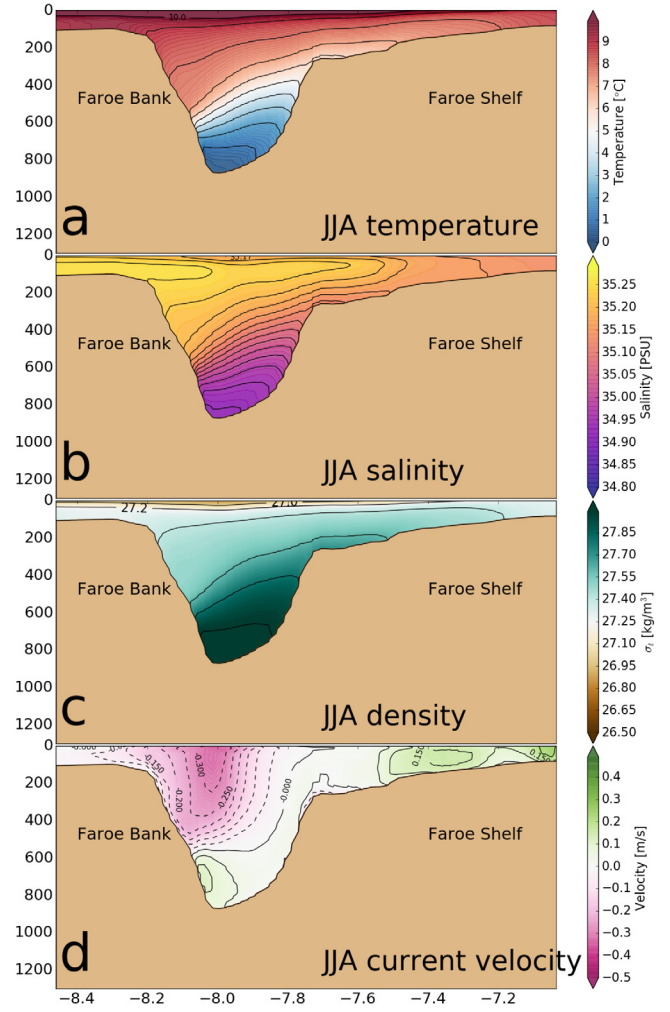

Fig. 4. Modeled average (a) temperature (one °C between lines), (b) salinity (0.025 psu between lines), (c) density (0.2 kg/m^3 between lines) and (d) velocity (northward component, 0.05 m/s between lines) for the June, July, August (JJA) summer season along the western section (WesternS) in Fig. 2. Similar plots for all seasons are available in the supplementary material.

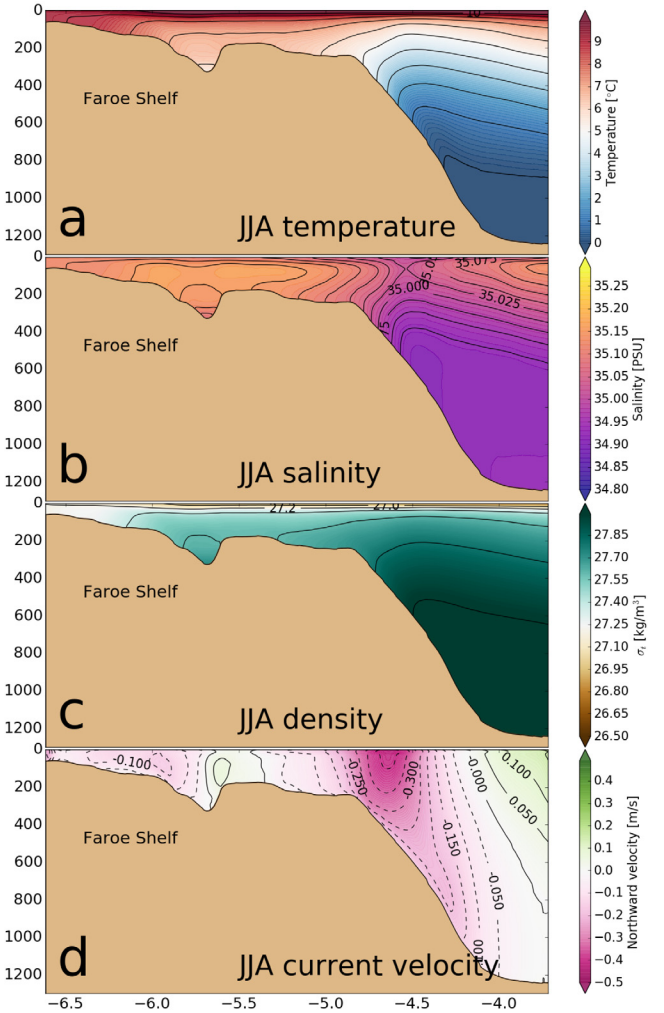

Fig. 5. Modeled average (a) temperature (one °C between lines), (b) salinity (0.025 psu between lines), (c) density (0.2 kg/m^3 between lines) and (d) velocity (northward component, 0.05 m/s between lines) for the June, July, August (JJA) season along the eastern section in Fig. 2. Similar plots for all seasons are available in the supplementary material.

34.92 PSU and a core of fresher water against the shelf only existing in the JJA and SON average (Figs. 5 and S7) indicating water of Arctic origin (Hansen and Østerhus, 2007; McKenna et al., 2016). Above the upper part of the Faroe shelf slope at 4.9°W to 4.2°W, the water is in general fresher, colder and flowing southwards (Figs. 5, 8 and 9). Comparing towards the observations (Figs. 8 and 9) the salinity is somewhat too low and the temperature is somewhat too high comparing to the model (Fig. 8c) and (Fig. 9c). Following the horizontal distribution of the temperature at 50 m depth (Figs. 10 and 11) this colder and fresher water seen in this section arrives from north of the Faroes and is thus mostly likely of EIC origin.

During February the temperature and salinity isolines from the model and the observations are tilting in opposite directions from 4.3°W and further east (Figs. 8a,d and 9a,d). This is in the model area where spurious currents occur in Fig. 3 at 4°W, induced by the boundary conditions in our model domain since they are not present in the lateral ocean forcing model domain (Figure S1). For the section during May (Fig. 9b,e), there appears to be a spatial bias where the salinity maximum in the model simulation is located at about 5.0°W the observations have a salinity maximum at 4.8°W.

The upper layers are dominated by MNAW (>7 °C) on the Faroe shelf side in the FSC, and the warmer and saltier NAW on the Scottish side, with some intrusion from below of the fresher and colder EIC above the Faroe shelf slope at ∼4.5°W. The strong summer (JJA) stratification (Fig. 5a,b) in the upper 50 m, breaks down during winter and spring (Figures S7 and S5).

The flow field along the eastern shelf Fig. 5d resembles the results obtained by ferry mounted ADCP by Rossby and Flagg (2012), despite the northward flow in model appears further west than in the study by Rossby and Flagg (2012); this is in the area with spurious currents. The salinity and temperature is in fair accordance with the literature (Hansen and Østerhus, 2007; McKenna et al., 2016; Rossby and Flagg, 2012), although the content of the fresher and colder water appears to be slightly exaggerated in the model and the salinity slightly underestimated as the core of the NAW is about 0.05 PSU below what is observed in Hansen and Østerhus (2007).

4.3. The on-shelf waters

4.3.1. The on-shelf annual mean currents

The annual mean currents from the barotropic flow in the model simulation (Fig. 3) captures the relatively strong clockwise

mean circulation in the coastal areas described amongst other by Larsen et al. (2008) and Rasmussen et al. (2014) and Fig. 1. The relatively strong residual flow around the southern tip of the southern most island towards the west may be noted, where velocities reach up to 0.6 m/s, and currents of similar strength as in Rasmussen et al. (2014). Similar mean velocities are also reached around the westernmost islands in fair agreement with previous numerical simulations (Rasmussen et al., 2014; Kragesteen et al., 2018). This relatively strong residual tidal current largely defines the CS which is within the 90 m contour line. As in Kragesteen et al. (2018) the tidal residual current is distinguishable between a northern, a central and a southern group of islands. The CS appears as areas with same temperature at all shown depths in Fig. 10 and as homogeneous water masses on the shelf in hydrographic sections in Figs. 4–9. The separation into several different areas of tidal residual currents is more obvious in Fig. 11 at 50 m depth.

On the OS there is a generally weaker, mean clockwise flow around the islands, on the order of 0.1 m/s or less, which is comparable with observations (Larsen et al., 2008). The OS tidal residual current is also visible at 7.4°W in Fig. 4d and at 6.1°W in Fig. 5d.

4.3.2. Outer shelf, western region

On the western shelf the model shows well mixed water masses in the CS water. Seen east of 7.2°W in Figs. 4a,b as well as the daily averages in Figs. 6 and 7. West of the CS, from 7.2°W to 7.6°W, which here identifies the FSF, and out to the shelf edge the model indicate more homogeneous water than in the observations in February (during the spin-up period), but the surface stratification develops through the spring in fairly good accordance with the observations (Eliasen et al., 2017b).

The section from the model in February and September are about one degree colder than the observations.

4.3.3. Outer eastern shelf, eastern banks

During winter and spring the water on the eastern shelf is vertically homogeneous (Figs. 8a,b,d,e and 9a,b,d,e), but in summer a surface stratification develops (Figs. 8c,f and 9c,f). It is only in proximity of land west of 6.6°W that the water column is mixed all year round.

Over the bank on the eastern shelf, the model has a small maximum in both salinity and temperature (Figs. 8 and 9a,b,c), which is weakly identifiable in the observations (Figs. 8 and 9d,e,f) and seasonal model mean (Fig. 5a,b and clearer identifiable during the other seasons in supplement Figure S5). Spatial plots of the temperature at 50 m depth (Fig. 10) indicate an inflow of MNAW intruding the eastern region from the FC to the north, in particular in spring and summer (Fig. 10). This water is overlaid by the summer stratification, and less visible at 5 m depth (Figs. 8 and 10). Observing the temperature anomaly in Fig. 11 in February at 5 m and 50 m depth and in June at 50 m depth the intrusion of MNAW occurs at the boundary between the OS and the EB in Fig. 2

In the trench separating EB from the OS at 5.6°W, the model has relatively cold and fresh water (Figs. 8 and 9). This is also seen in the observations, however not visible in the contour plots, since this is only a single station.

The residual current (Figs. 3 and 5d) on the inner part of the eastern shelf is southward, and the region close to the shelf edge is also dominated by southward flow as discussed in Section 4.2.2 in good accordance with the clockwise current described by Hansen and Østerhus (2007) and Larsen et al. (2008, e.g.). However, at the inner edge of the bank on the eastern shelf (5.7°W), the model has a residual northward flow, which is evident in current profiles obtained by ferry crossing this area regularly (Rossby and Flagg, 2012). In the model this current disappears during DJF (Figure S8).

Table 1
Annual temperature averages from observations and model simulation and Pearson correlation coefficient p between observed and modeled temperature anomalies at the three coastal stations.

Annual mean temperatures (°C):			
Station	Sk	Oy	Ei
Observation	8.33	8.32	8.20
Model	7.51	7.52	7.48
Bias	0.82	0.8	0.72
Pearson correlation coefficient (p):			
p	0.995	0.996	0.98

4.4. Seasons on the Faroe shelf

4.4.1. Temporal variations on the shelf

Annual timeseries of the simulated difference between the near bottom and near surface temperature are compared to observations and shown in Fig. 12. As in Eliasen et al. (2017a) the temperature timeseries are used to separate WR and EB (station W and S in Fig. 2). Here the model captures the strong summer stratification on the EB at station S. The model captures fairly well the annual variation, as well as most of the short term variations, although, there is some bias between the observations and the model. For station W the Pearson correlation coefficient is 0.71, the covariance is 0.23 for the period from 3rd of January to 17th of September. For station S the correlation and the covariance are 0.97 and 2.06, respectively.

For the EB the stratification occurs in the beginning of May (Fig. 12a). From Figs. 8 and 9 it is clear that this is the case for the entire EB and not just the local station S. The observations in Fig. 12a indicate a more gradual gradient change in the stratification in May than the model setup reproduces. For the WR the stable stratification occurs later, in June, and is less significant; thus not seen in the section Figs. 6 and 7 until the section from early September.

During the summer season there is a bias of ΔT up to 1 °C on the EB at station S and up to 2 °C on the WR station W (Fig. 12).

4.5. Coastal timeseries

The temperature time series are available from the three coastal stations: Sk, Oy and Ei (Fig. 2). The model displays vertically well mixed water on the CS (Figs. 4–8) through all seasons (Figure S5).

The annual mean temperature in the model is generally about 0.8 °C colder than the observations (Table 1), but this bias varies both with time and spatially (Fig. 13). At the two stations with tidally well mixed water, Oy and Sk (Figs. 13a and b) the model slightly underestimates the temperature in particular in winter, while at the more protected station Ei the bias is more constant throughout the year (Fig. 13c). See location in Fig. 2b.

Comparison with observations at the southernmost islands are similar to the two tidally well mixed stations (Oy and Sk), while comparisons with observations from the islands in the northeast shows a good agreement between model and data in winter, but the model is slightly warmer in summer (not shown).

The capability of the model to simulate the short term variability is investigated by calculating the anomaly between the daily temperature and a monthly 30 day running mean for the three coastal stations (Fig. 14). The model performance at all three coastal stations is quite high as demonstrated by the Pearson correlation coefficient p in Table 1.

At station Sk (Fig. 14a) there is an event in March and one in August where the model under and over-estimates the temperature respectively. Otherwise the model captures the variation to

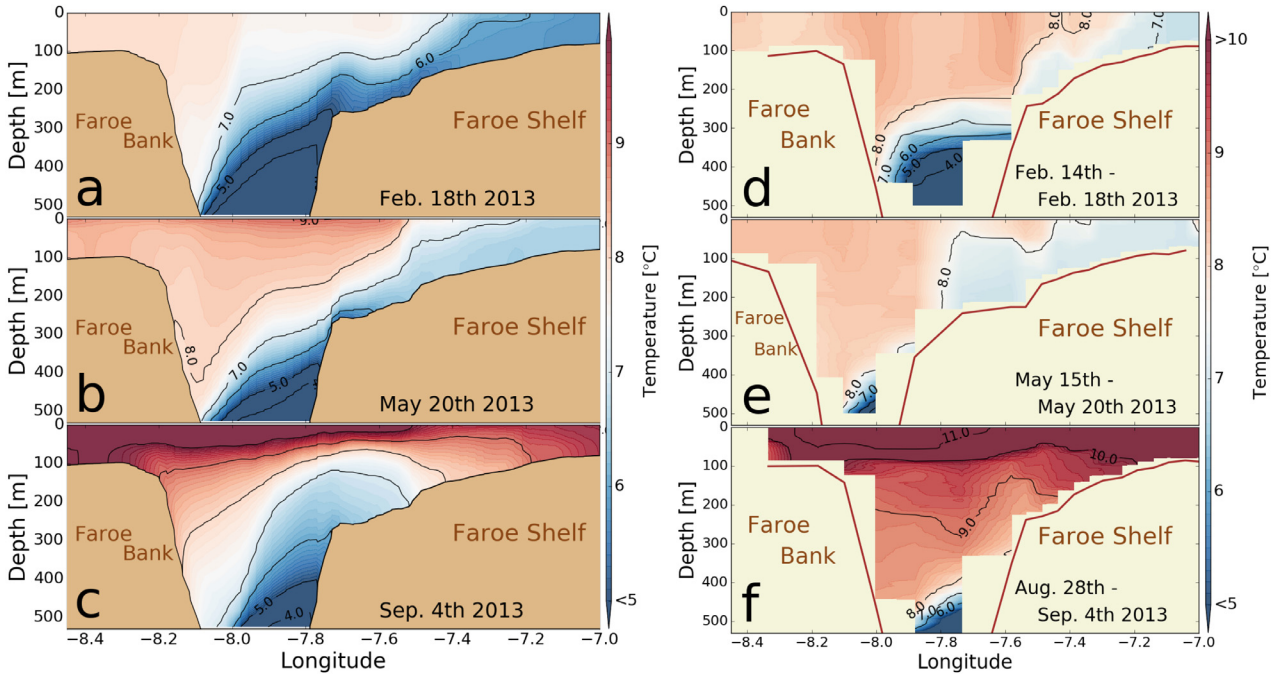

Fig. 6. a,b,c: Daily temperature averages from the model at section WesternS (Fig. 2). d,e,f: Temperature from observations at section WesternS obtained by FAMRI during cruises in February, May and August 2013 (Fig. 2).

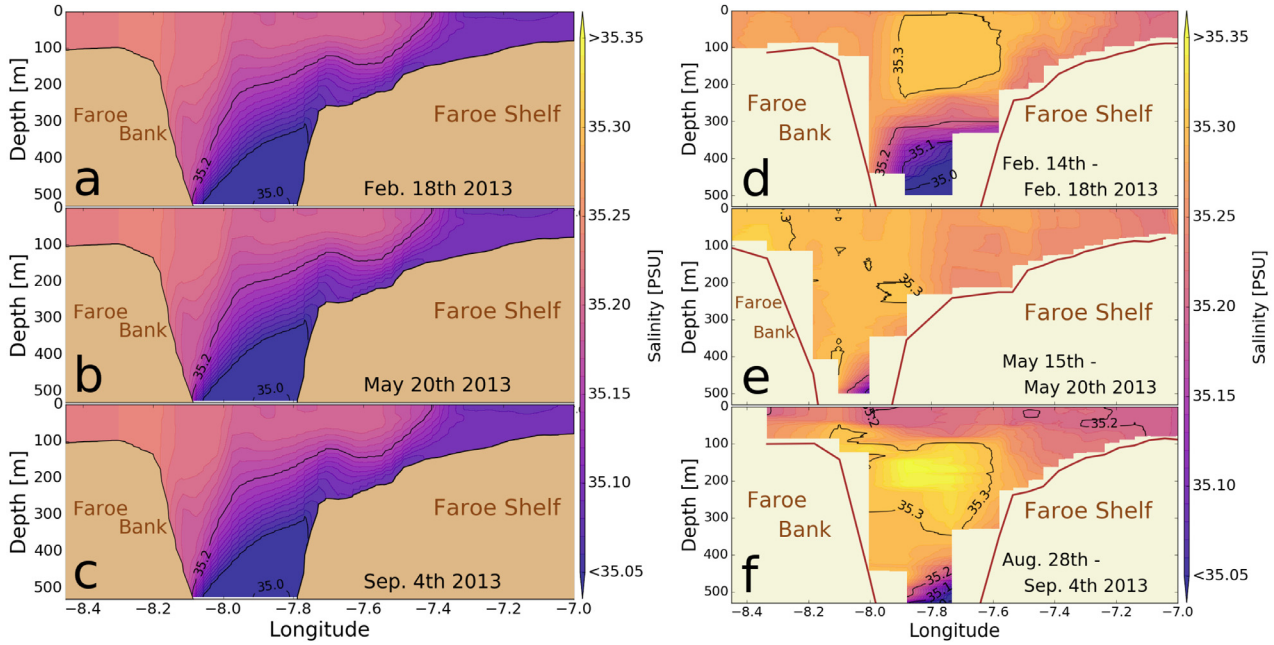

Fig. 7. a,b,c: Daily salinity averages from the model at section WesternS (Fig. 2). d,e,f: Salinity from observations at section WesternS obtained by FAMRI during cruises in February, May and August 2013 (Fig. 2).

a high degree. For the station Oy (Fig. 13b) the discrepancies are even less, there is no significant difference between the model and observed variation. There is a small period in August where the model slightly overestimates the temperature variation.

For station Ei (Fig. 1c) the agreement between model and observations is generally good, except for some low temperature events seen in the observations in the summer months June and July.

Generally, the model underestimates the salinity with 0.02–0.17 PSU when compared to the observations from station Sk, with the largest deviation in the first half year of the simulation (Fig. 16). The lower salinities are also apparent when compared with the hydrographic sections (Figs. 7 and 9).

5. Discussion

The FarCoast800 model setup reproduced the hydrodynamics on and off the Faroe shelf reasonably well. The temperature variations were reproduced with a very high correlation for the coastal stations compared to observations (Table 1). Similarly the current velocities were also well reproduced, and both the inner

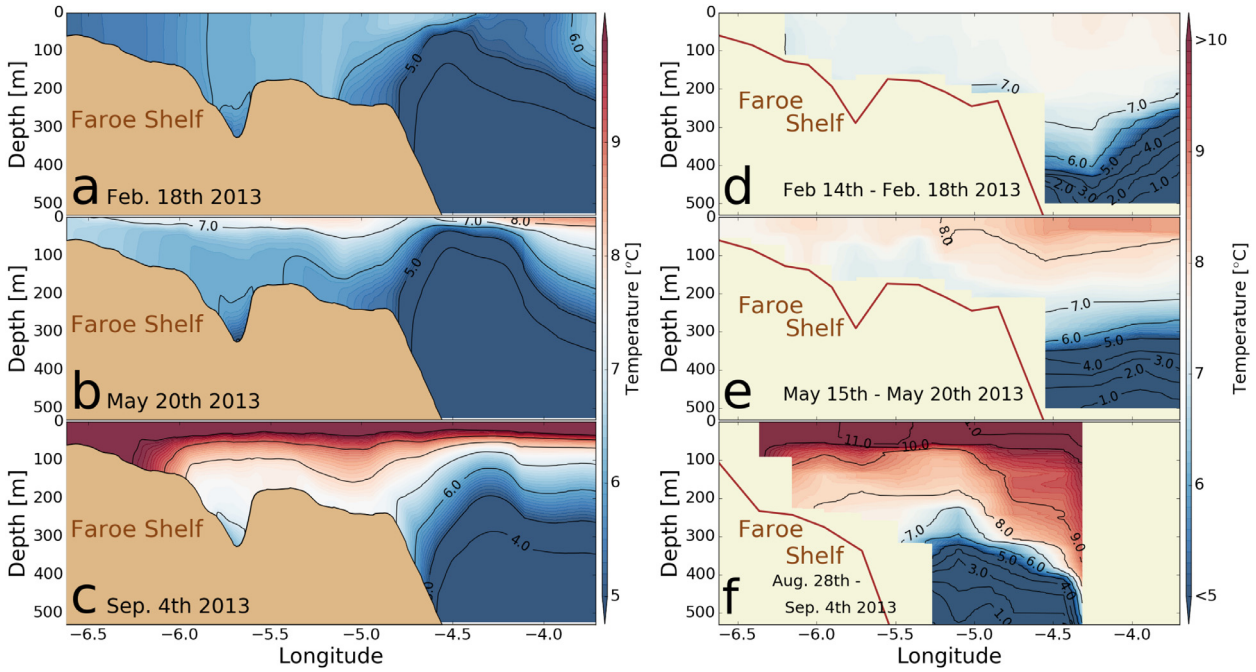

Fig. 8. a,b,c: Daily temperature averages from the model at section EasternS (Fig. 2). d,e: Temperature from observations from the Section EasternS obtained by FAMRI in February and May 2013. f: Temperature from section SouthernS a bit south of EasternS from FAMRI during cruise in August 2013 (Fig. 2).

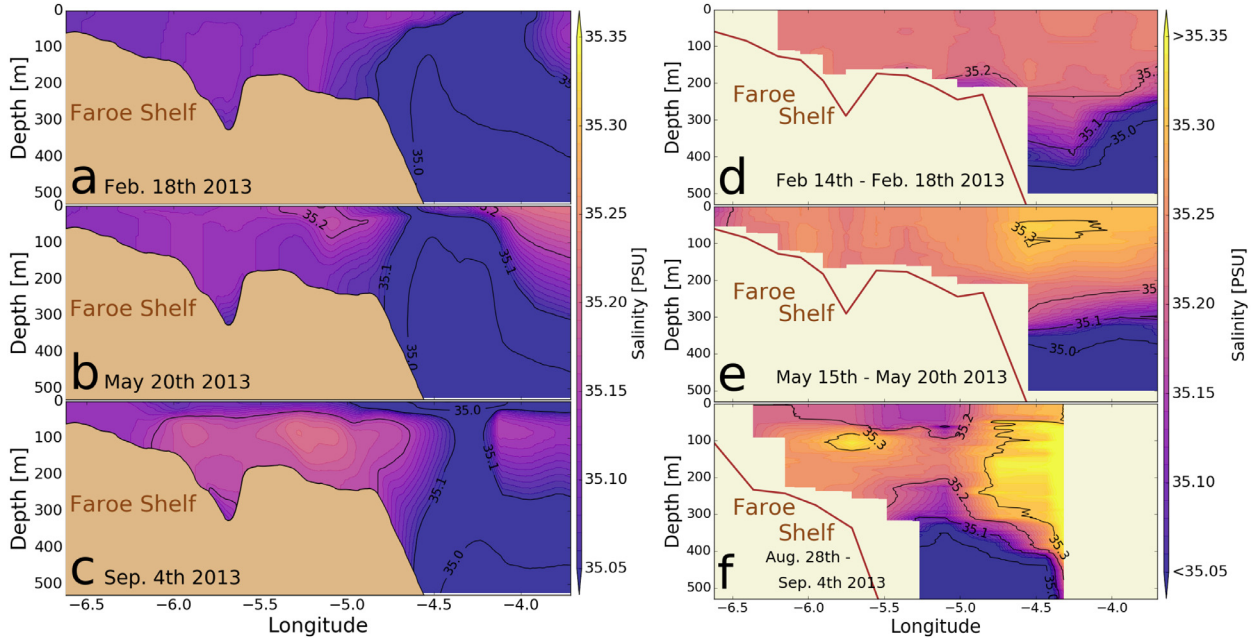

Fig. 9. a,b,c: Daily salinity averages from the model at section EasternS (Fig. 2). d,e: salinity from observations at the Section EasternS obtained by FAMRI in February and May 2013. f: salinity from section SouthernS a bit south of EasternS from FAMRI during cruise in August 2013 (Fig. 2).

and outer clockwise residual currents had compatible velocities to earlier studies (Larsen et al., 2008, 2009; Hansen et al., 2017).

In Section 4.1 we touched upon the model circulation, in particular along the eastern part of the model domain perimeter but also along the northern part of the model domain perimeter being rather spurious (Fig. 3). This is from the inconsistency of the bathymetry between the coarser 4 km model and the 800 meter simulation (Figure S1). However as stated through the results section this seems not to affect the obtained circulation on the shelf area, which is our main interest. The results showed reasonably realistic values for the circulation in the CS and we saw the tidal residual circulation in the barotropic flow in Fig. 3. Only on the easternmost part of the EasternS in the FSC we observed a large inconsistency between the model and the observations in velocities 5d. Nonetheless, this together with the recirculation on the northern boundary of the domain, implies that some caution most be taken in the interpretation of the flow of Atlantic water, entering the northern shelf and continuing into the southward flowing water on the eastern shelf as this amount could be exaggerated. The spurious flow along the boundary may also imply an erroneous pressure field as mentioned in Lien et al. (2013). In our case this could reduce the eastern flowing branch of Atlantic water into the Norwegian Sea and instead increase the amount of Atlantic water that is flowing onto the eastern shelf.

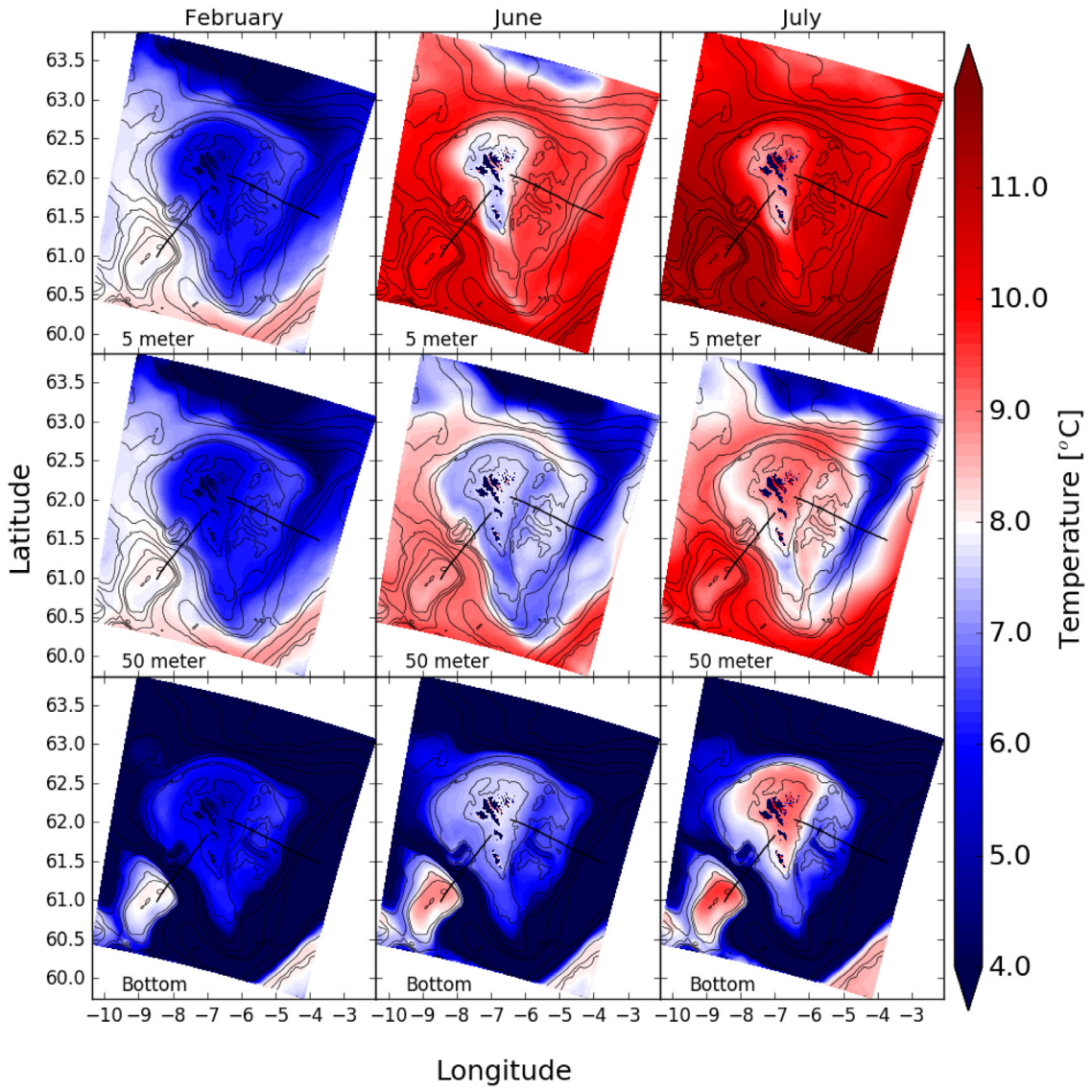

Fig. 10. Modeled temperature (°C, colorbar) at 5 meters depth (top), and 50 meters depth (middle) and in the bottom layer (last) in February, June, and July. Solid lines are depth contours at 100 m, 300 m, 500 m, 700 m, 1000 m, 1500 m, 2000 m, 3000 m. The black lines are the WesternS and the EasternS respectively.

The model domain is balancing the inflow and outflow and thus introducing the spurious currents along the northern and eastern model domain boundaries. However since our main interest is the Faroe shelf itself, it seems that the FarCoast800 model setup handles this issue quite well and is adjusted to simulate realistic conditions for the currents once reaching the central area of the model domain.

The results in Sections 4.2 and 4.3 indicate that the model performance by FarCoast800 is quite realistic on the shelf. Only during February, which is part of the spin-up period, the modeled salinity and the modeled temperature (Figs. 8a and 9a) disagree with observations. However, there is clearly a bias between the model and the observations when considering the absolute values of both temperature and salinity during the entire sample year. Due to the bias being quite persistent, this is an indication that the model setup and the dynamics are well captured and the issue is mainly from the boundary forcing. Thus the bias in temperature and in particular salinity may, at least partly, be traced back to the climatology (SODA) used as boundary condition in the SWIM model. Improving this would probably make it possible to compare the absolute values of temperature and salinity in Section 4.5.

The panel plot in Fig. 10, showing the monthly averages of the temperature for February, June and July at three different depths, clearly supports the assumption of the difference in dynamics of the OS and EB (Fig. 2). In the bottom layer (Fig. 10) the horizontal temperature gradient is strongest in the summer months, this demonstrates the dominance of atmospheric forcing in the shallow areas. Furthermore, at 50 meters depth the model indicates that water from the west (MNAW) flows northeastward around the shelf and flushes directly onto the EB from the northwest.

The model indicates that water, originating from the EIC, on the eastern Faroe shelf slope, flows in a relatively thin layer into the trenches deeper than 140 m on the eastern shelf (Fig. 10). There might be a week signal of some inflow along the banks in the observed sections in February and May (Fig. 8, at 5.7°W). Otherwise the observational evidence are scarce, except for a temperature series near bottom at the inner slope of the this trench showing an abrupt drop in temperature of 3–4 °C, and thereafter in periods, a tidal variation indicating that a temperature front is moving across this location. (K. M. H. Larsen, FAMRI, 2019, pers. comm., Hansen (2018))

The results also indicate a small intrusion of water from the eastern shelf being recirculated onto the western side of the

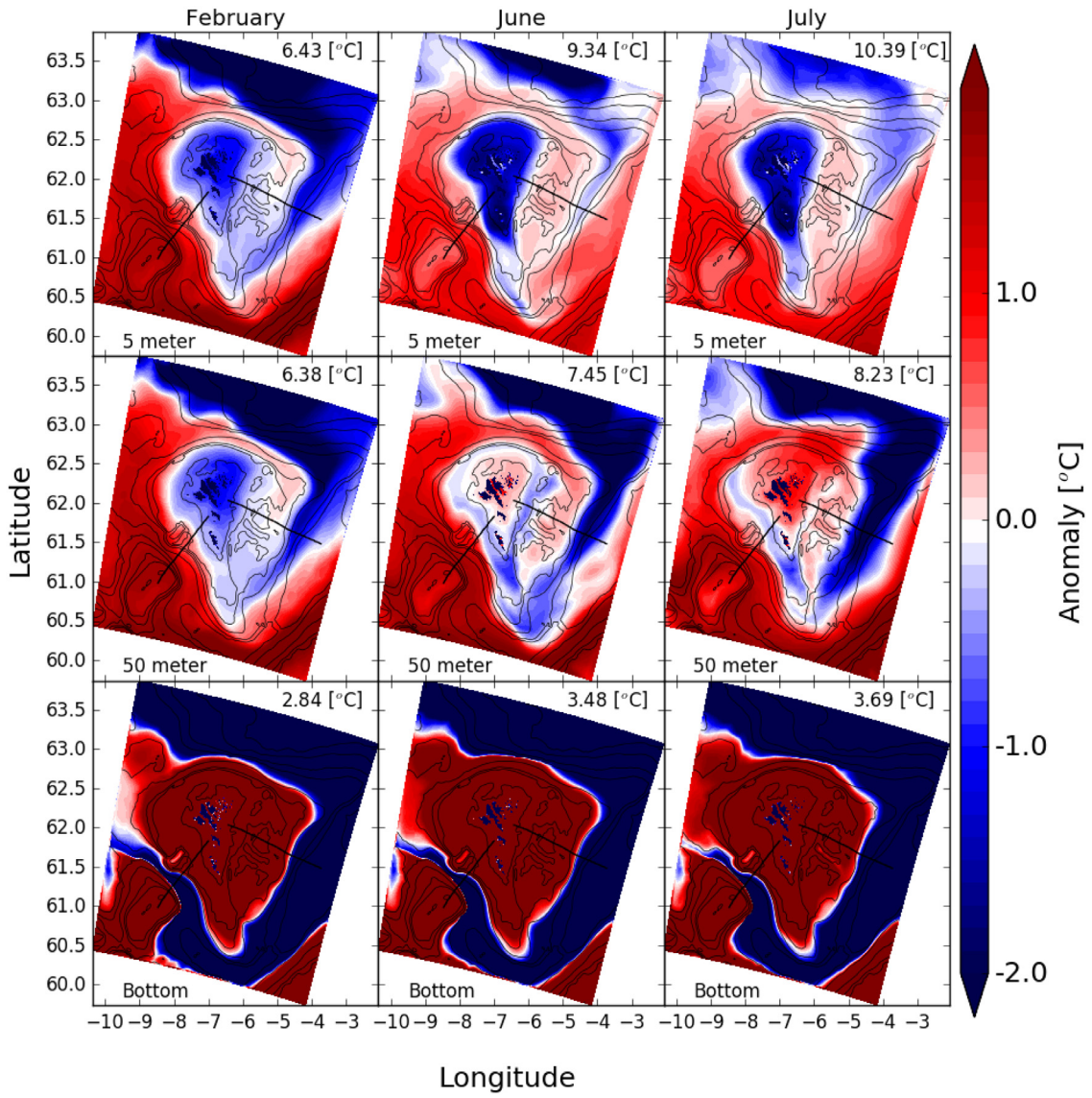

Fig. 11. Modeled temperature anomaly (°C, colorbar) at 5 meters depth (top), and 50 meters depth (middle) and in the bottom layer (last) in February, June, and July. Temperature anomaly is relative to monthly mean temperature shown in upper right corner of each plot. Solid lines are depth contours at 100 m, 300 m, 500 m, 700 m, 1000 m, 1500 m, 2000 m, 3000 m. The black lines are the WesternS and the EasternS respectively.

shelf across the southern part of the shelf (Fig. 3). There is some disagreement in how large this recirculation is in volume (Rossby and Flagg, 2012; Hansen et al., 2017). From the model simulation, it seems possible, that the WR and OS are fed from below by the colder water masses from FC and EIC through the southeastern part of the shelf (Fig. 11 at 50 meter depth and S3).

Again looking at Fig. 10 bottom layer, there is also a temperature gradient, between the central area of the sound between the largest islands, and the surrounding CS, indicating a locked bottom layer in the sound during June and July which is observed by Simonsen et al. (2018) and Hansen (1990) in the sound, although this has not been quantified by a model simulation prior to this study. The upper layers are controlled by atmosphere to a strong degree and below 50 meter depth we observe the oceanographic influence to become more dominant. The on-shelf water masses are resupplied by the surrounding ocean waters masses where mechanical energy drives the exchange (Eliasen et al., 2017a; Simpson and Sharples, 2012). Buoyancy driven input from atmosphere is dominant for shelf water, alongside fresh water input and tidal direct forcing from wind and waves (Eliasen et al., 2017a; Simpson and Sharples, 2012).

The seasons on the Faroe shelf are defined through temperature changes and the changes observed through stratification (Eliasen et al., 2017a) which are clearly visible in Fig. 12. During winter the shelf water is unstratified and there is no vertical temperature gradient neither in the WR nor the EB (Figs. 6a and 8a). The spring season is defined as to when the stratification on the shelf begins (Eliasen et al., 2017b). The temperature bias in Fig. 12 is greatest in the bottom layer of the model and is most likely influenced by the boundary conditions (Figure not shown). Since the setup favors higher resolution in the upper 50 m, our applied grid stiffness may introduce various levels of horizontal pressure gradient errors and then non-real velocities as observed in the FBC (Beckmann and Haidvogel, 1993; Haney, 1991).

However, considering the long term salinity variations in the observations at station Sk (Fig. 15), the salinity was generally higher than obtained by the model in all years back to the beginning of the record in year 1996 (Larsen et al., 2008). The observation shows a clear seasonal variation with lower values in the winter, though not as low as seen in our simulation in the period back to year 2000 (Larsen et al., 2008). In mid 2013 the observed seasonal decline started relatively early and ended

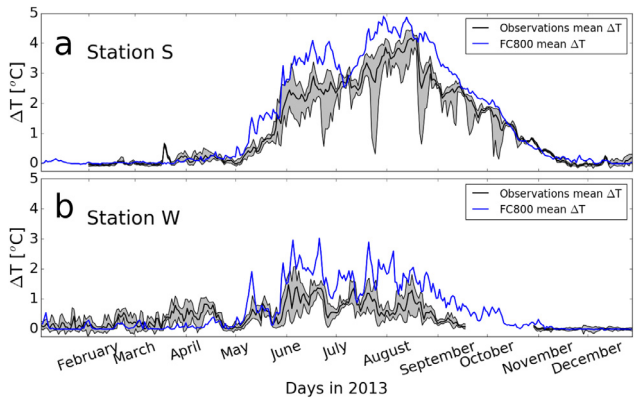

Fig. 12. Surface to bottom temperature difference at stations S (a) and W (b). The black line is daily mean, while the gray areas indicate daily minimum and maximum measured temperature differences and blue lines are daily mean from the numerical model. (For interpretation of the references to color in this figure legend, the reader is referred to the web version of this article.)

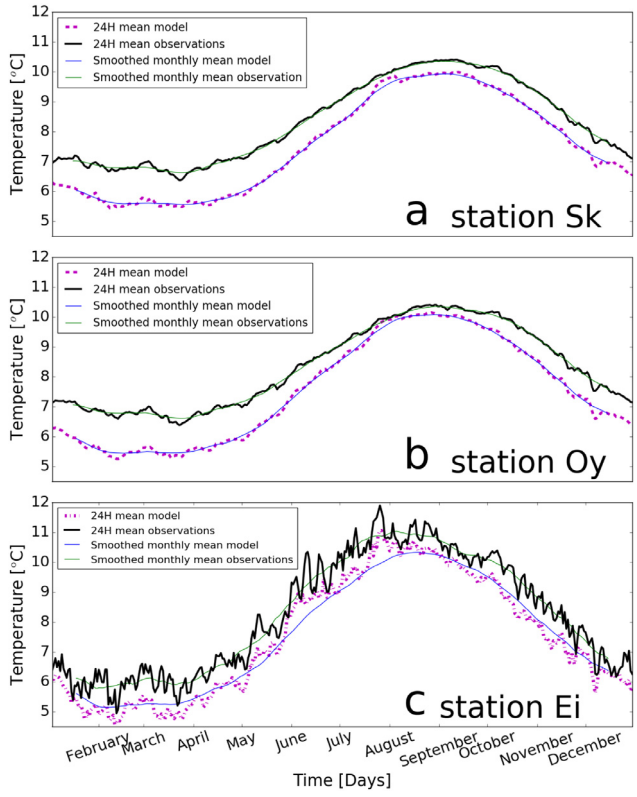

Fig. 13. Daily mean (thick line) and monthly mean (thin line) from the model (magenta and blue) and observations (black and green) at the central shelf stations Sk (a), Oy (b), and Ei (c). See Fig. 2 for locations. (For interpretation of the references to color in this figure legend, the reader is referred to the web version of this article.)

in the lowest winter minimum seen in the record until then. In the following three years the observed salinity stayed at the level obtained in the simulation until the winter 2016–17, when the salinity declined further to a level of order 0.1 PSU below our model results. In the multiyear simulation by Rasmussen et al. (2014), they obtained a fairly good agreement in salinity in the first years of their simulations, but in the last years of the simulation the model was not able to follow the increasing salinity, which they explained was related to their boundary forcing.

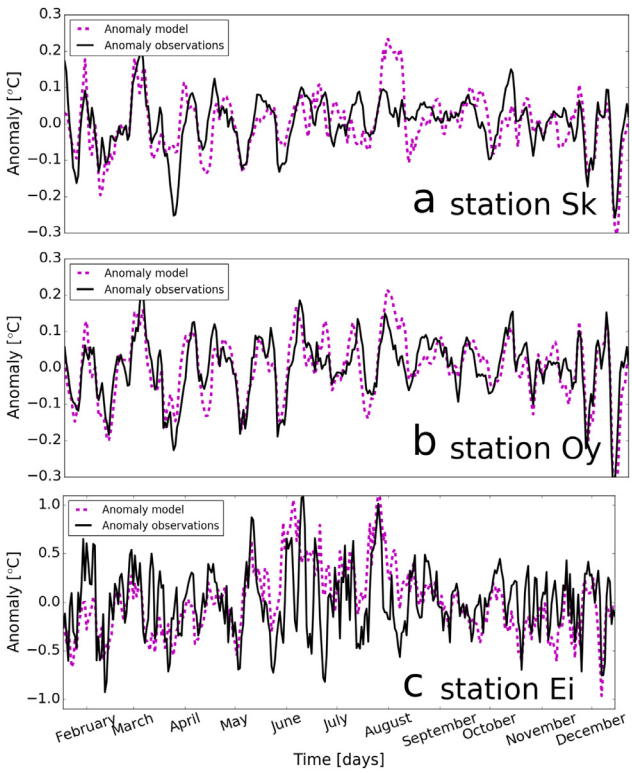

Fig. 14. Temperature anomalies at stations Sk (a), Oy (b) and Ei (c) (Fig. 2) estimated by subtracting 30 day running mean from the daily mean temperatures in Fig. 13. Note different vertical scale in the bottom plot.

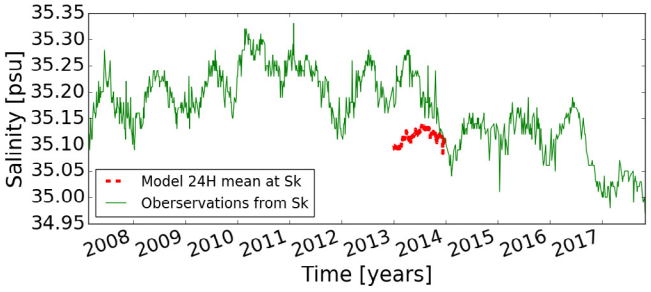

Fig. 15. Salinity at station Sk Fig. 2.

These long-term variations seen in the observed salinity are of lateral origin Larsen et al. (2009). The salinity variations are likely regulated by the strength of the North Atlantic Subpolar Gyre, which influences the strength of the relative amount of MNAW and the more saline NAW water is flowing into the area (Hátún et al., 2005). This dynamic feature of the North Atlantic that most probably is influencing our region of interest is omitted in our simulation. Here, as mentioned, we adopt the lateral boundary forcing from the SVIM model, which again applies a climatology along its lateral boundary in the Atlantic in 2013 (Section 3.1).

6. Concluding remarks

Our main conclusions are firstly that in order to be able to simulate day to day upper ocean variations a highly resolved atmospheric model is important, as we found high correlations between observations and model output. Secondly we can conclude that there is a difference of the feeding of water onto the eastern region and the western region controlled by the

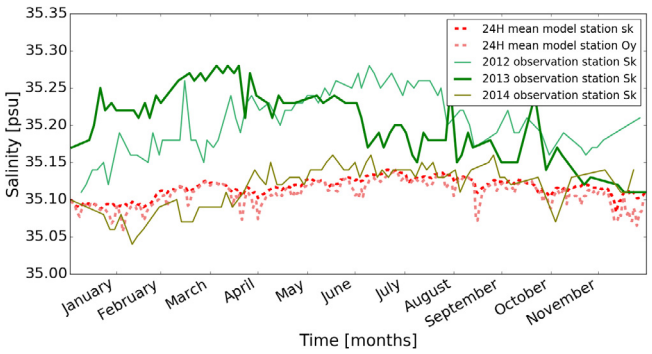

Fig. 16. Annual salinity observations 2012–2014 against FC800 from 2013.

large scale upper ocean currents that can be recognized through temperature differences on the shelf.

The 800 meter resolution of FarCoast800 is highly capable of reproducing the short term variations on the upper shelf. Our validation show that a high resolution atmospheric forcing is significant in order to get a realistic simulation.

This paper shows that the FarCoast800 model setup has good performance on and around the Faroe shelf, even though the model flow in the off-shelf area is highly constrained by the boundary conditions and the set-up, where enhanced resolution for the upper 50 meters is preferred.

In a future model based salmon louse prediction and contingency system for the Faroe Islands the model domain can improve the predictions of sea lice infestation pressure as in Sandvik et al. (2016). Since the quality of such a louse dispersion model will depend of the quality of the underlying system, it is imperative that the ocean model is of high quality.

7. Abbreviations

ADCP	Acoustic Doppler Current Profiler
CS	Central Shelf
EIC	East Icelandic Current
EB	Eastern Banks
FB	Faroe Bank
FBC	Faroe Bank Channel
FBCO	Faroe Bank Chanel Overflow
FC	Faroe Current
FMRI	Faroe Marine Research Institute
FSC	Faroe Shetland channel
FSF	Faroe Shelf Front
GLS	Generic Length Scale
HYCOM	3D HYbrid Coordinate Ocean Model
IFR	Iceland Faroe Ridge
MNAW	Modified North Atlantic Water
NADW	North Atlantic Deep Water
NAW	North Atlantic Water
NSDW	Norwegian Sea Deep Water
OPW	Office for Public Works
OS	Outer Shelf
ROMS	Regional Ocean Modeling System
SFC	Southern Faroe Current
SODA	Simple Ocean Data Assimilation
SSC	Scottish Slope Current
SVIM	Nordic Seas 4 km numerical ocean model hindcast archive
WR	Western Region
WRF	Weather Research and Forecasting model
WTB	Wyville Thomson Basin

Declaration of competing interest

The authors declare that they have no known competing financial interests or personal relationships that could have appeared to influence the work reported in this paper.

Acknowledgments

The timeseries and hydrographic data provided by Faroe Marine Research Institute and Office for Public Works in the Faroes (www.landsverk.fo) is very much appreciated.

Thanks to Lars Asplin, Institute of Marine Research, Norway, for providing the network and for the general introduction to ROMS.

Thanks to the two anonymous reviewers for the highly appreciated constructive feedback.

This paper is part of the PhD project by SVE, which is financially supported by Statoil Faroes, Mowi Faroe Islands , P/F Bakkafrost and the Faroese Research Council (Grant no. 0445).

Appendix A. Supplementary data

Supplementary material related to this article can be found online at https://doi.org/10.1016/j.rsma.2020.101475. Here we include all of the seasonal section plots for both sections WesternS and EasternS, as well as average

References

Beaird, N.L., Rhines, P.B., Eriksen, C., 2016. Observations of seasonal subduction at the iceland-faroe front. J. Geophys. Res.: Oceans 121 (6), 4026–4040. http://dx.doi.org/10.1002/2015JC011501, URL: https://agupubs.onlinelibrary.wiley.com/doi/abs/10.1002/2015JC011501.

Beckmann, A., Haidvogel, D.B., 1993. Numerical simulation of flow around a tall isolated seamount. part I: Problem formulation and model accuracy. J. Phys. Oceanogr. 23 (8), 1736–1753. http://dx.doi.org/10.1175/1520-0485(1993)023<1736:NSOFAA>2.0.CO;2, URL: arXiv:https://journals.ametsoc.org/jpo/article-pdf/23/8/1736/4423464/1520-0485(1993)023_1736_nsofaa_2_0_co_2.pdf.

Carton, J., Chepurin, G., Cao, X., Giese, B., 2000. A simple ocean data assimilation analysis of the global upper ocean 1950 95. part I: Methodology. J. Phys. Oceanogr. 30, 294–309. http://dx.doi.org/10.1175/1520-0485(2000)030<0294:ASODAA>2.0.CO;2.

Carton, J.A., Giese, B.S., 2008. A reanalysis of ocean climate using simple ocean data assimilation (SODA). Mon. Weather Rev. 136 (8), 2999–3017. http://dx.doi.org/10.1175/2007MWR1978.1, URL: arXiv:https://doi.org/10.1175/2007MWR1978.1.

Chapman, D.C., 1985. Numerical treatment of cross-shelf open boundaries in a barotropic coastal ocean model. J. Phys. Oceanogr. 15, 1060–1075. http://dx.doi.org/10.1175/1520-0485(1985)015.

Chassignet, E.P., Hurlburt, H.E., Smedstad, O.M., Halliwell, G.R., Hogan, P.J., Wallcraft, A.J., Baraille, R., Bleck, R., 2007. The HYCOM (hybrid coordinate ocean model) data assimilative system. J. Mar. Syst. 65 (1), 60–83. http://dx.doi.org/10.1016/j.jmarsys.2005.09.016, Marine Environmental Monitoring and Prediction.

Dam, P.M., 2019. Statistics FAROE ISLANDS. URL: https://hagstova.fo/en/economy/international-trade/exports-goods.

Davidsen, E., Førland, E., Madsen, H., 1994. Orographically enhanced proecipitation on the faroe islands. In: Kern-Hansen, C., Rosbjerg, D., Thomsen, R. (Eds.), Nordic Hydrological Conference 1994. Nordic Hydrological Program (NHP) Report, number 34, Nordic Association for Hydrology, Tórshavn, Faroe Islands, pp. 229–239.

Egbert, G., Erofeeva, S., 2002. Efficient inverse modeling of Barotropic ocean tides. J. Atmos. Ocean. Technol. 19, 183–204. http://dx.doi.org/10.1175/1520-0426(2002)019<0183:EIMOBO>2.0.CO;2.

Eliasen, S.K., Hansen, B., Larsen, K.M.H., Hátún, H., 2016. The exchange of water between the Faroe Shelf and the surrounding waters and its effect on the primary production. J. Mar. Syst. 153, 1–9. http://dx.doi.org/10.1016/j.jmarsys.2015.08.004.

Eliasen, S.K., Hátún, H., Larsen, K.M.H., Hansen, B., Rasmussen, T.A.S., 2017a. Phenologically distinct phytoplankton regions on the Faroe Shelf - identified by satellite data, in-situ observations and model. J. Mar. Syst. 169, 99–110. http://dx.doi.org/10.1016/j.jmarsys.2017.01.015.

Eliasen, S.K., Hátún, H., Larsen, K.M.H., Jacobsen, S., 2017b. Faroe shelf bloom phenology – the importance of ocean-to-shelf silicate fluxes. Cont. Shelf Res. 143, 43–53. http://dx.doi.org/10.1016/j.csr.2017.06.004.

Eliasen, S.K., Hátún, H., Larsen, K.M.H., Vang, H.B.M., Rasmussen, T.A.S., 2019. The faroe shelf spring bloom onset explained by a 'Critical Volume Hypothesis'. J. Mar. Syst. 194, 91–101. http://dx.doi.org/10.1016/j.jmarsys.2019.02.005.

Flather, R., 1976. A tidal model of the northwest European continental shelf. Mem. Soc. R. Sci. Liege 10, 141–164..

Haidvogel, D., Arango, H., Budgell, W., Cornuelle, B., Curchitser, E., Lorenzo, E., Fennel, K., Geyer, W., Hermann, A., Lanerolle, L., Levin, J., McWilliams, J., Miller, A., Moore, A., Powell, T., Shchepetkin, A., Sherwood, C., Signell, R., Warner, J., Wilkin, J., 2008. Ocean forecasting in terrain-following coordinates: Formulation and skill assessment of the regional ocean modeling system. J. Comput. Phys. 227, 3595–3624. http://dx.doi.org/10.1016/j.jcp.2007.06.016.

Haney, R.L., 1991. On the pressure gradient force over steep topography in sigma coordinate ocean models. J. Phys. Oceanogr. 21 (4), 610–619. http://dx.doi.org/10.1175/1520-0485(1991)021<0610:OTPGFO>2.0.CO;2, URL: arXiv:https://journals.ametsoc.org/jpo/article-pdf/21/4/610/4422471/1520-0485(1991)021_0610_otpgfo_2_0_co_2.pdf.

Hansen, B., 1990. Oxygentrot og útskifting íbotnvatninum á føroyskum gáttarfiròum. Fiskirannsóknir 6, 188–258.

Hansen, B., 2018. Botnhitin kring Føroyar. In: Faroe Marine Research Institute. Smárit, number 03, Havstovan, Tórshavn, Faroe Islands, pp. 1–22.

Hansen, B., Hátún, H., Kristiansen, R., Olsen, S.M., Østerhus, S., 2010. Stability and forcing of the Iceland-Faroe inflow of water, heat,and salt to the Arctic. Ocean Sci. 6, 1013–1026. http://dx.doi.org/10.5194/os-6-1013-2010.

Hansen, B., Húsgarò Larsen, K.M., Hátún, H., Østerhus, S., 2016. A stable faroe bank channel overflow 1995–2015. Ocean Sci. 12 (6), 1205–1220. http://dx.doi.org/10.5194/os-12-1205-2016, URL: https://www.ocean-sci.net/12/1205/2016/.

Hansen, B., Østerhus, S., 2000. North atlantic-nordic seas exchanges. Prog. Oceanogr. 45, 109–208.

Hansen, B., Østerhus, 2007. Faroe bank channel overflow 1995–2005. Prog. Oceanogr. 75, http://dx.doi.org/10.1016/j.pocean.2007.09.004.

Hansen, B., Poulsen, T., Húsgarò Larsen, K.M., Hátún, H., Østerhus, S., Darelius, E., Berx, B., Quadfasel, D., Jochumsen, K., 2017. Atlantic water flow through the faroese channels. Ocean Sci. 13 (6), 873–888. http://dx.doi.org/10.5194/os-13-873-2017.

Hátún, H., 2004. The Faroe Current (Ph.D. thesis). University of Bergen/Faroe Marine Research Institute.

Hátún, H., Sandø, A.B., Drange, H., Hansen, B., Valdimarsson, H., 2005. Influence of the atlantic subpolar gyre on the thermohaline circulation. Science 309, 1841–1843.

Huserbråten, M., Moland, E., Albretsen, J., 2018. Cod at drift in the North Sea. Prog. Oceanogr. 167, http://dx.doi.org/10.1016/j.pocean.2018.07.005.

Jacobsen, S., Gaard, E., Larsen, K.M.H., Eliasen, S.K., Hátún, H., 2018. Temporal and spatial variability of zooplankton on the Faroe shelf in spring 1997–2016. J. Mar. Syst. 177, 28–38. http://dx.doi.org/10.1016/j.jmarsys.2017.08.004.

Kragesteen, T.J., Simonsen, K., Visser, A.W., Andersen, K.H., 2018. Identifying salmon lice transmission characteristics between faroese salmon farms. Aquac. Environ. Interact. 10, 49. http://dx.doi.org/10.3354/aei00252.

Larsen, K.M., Hansen, B., Svendsen, H., 2008. Faroe shelf water. Cont. Shelf Res. 28 (14), 1754–1768. http://dx.doi.org/10.1016/j.csr.2008.04.006.

Larsen, K.M., Hansen, B., Svendsen, H., 2009. The faroe shelf front: Properties and exchange. J. Mar. Syst. 78 (1), 9–17. http://dx.doi.org/10.1016/j.jmarsys.2009.02.003.

Lien, V., Gusdal, Y., Albretsen, J., Melsom, A., Vikebø, F., 2013. Evaluation of a nordic seas 4 km numerical ocean model archive. Fisken og Havet 7, 7:79.

Marchesiello, P., McWilliams, J., Shchepetkin, A., 2001. Open boundary conditions for long-term integration of regional oceanic models. Ocean Model. 3, 1–20. http://dx.doi.org/10.1016/S1463-5003(00)00013-5.

McKenna, C., Berx, B., Austin, W., 2016. The decomposition of the faroe-shetland channel water masses using parametric optimum multi-parameter analysis. Deep Sea Res. Part I 107, 9–21. http://dx.doi.org/10.1016/j.dsr.2015.10.013.

Myksvoll, M., Sandvik, A., Albretsen, J., Asplin, L., Johnsen, I., Karlsen, O., Kristensen, N., Melsom, A., Skardhamar, J., Ådlandsvik, B., 2018. Evaluation of a national operational salmon lice monitoring system—From physics to fish. PLOS ONE 13, e0201338. http://dx.doi.org/10.1371/journal.pone.0201338.

Myksvoll, M., Sandvik, A., Skaròhamar, J., Sundby, S., 2012. Importance of high resolution wind forcing on eddy activity and particle dispersion in a norwegian fjord. Estuar., Coast. Shelf Sci. 113, 293–304. http://dx.doi.org/10.1016/j.ecss.2012.08.019.

Patursson, E.J., Simonsen, K., Visser, A.W., Patursson, Ø., 2017. Effect of exposure on salmon lice lepeophtheirus salmonis population dynamics in faroese salmon farms. Aquac. Environ. Interact. 9, 33–43.

Rasmussen, T., Olsen, S.M., Hansen, B., Hátún, H., Larsen, K.M., 2014. The faroe shelf circulation and its potential impact on the primary production. Cont. Shelf Res. 88, 171–184. http://dx.doi.org/10.1016/j.csr.2014.07.014.

Rossby, T., Flagg, C.N., 2012. Direct measurement of volume flux in the faroe-shetland channel and over the iceland-faroe ridge. Geophys. Res. Lett. 39 (7), http://dx.doi.org/10.1029/2012GL051269.

Sandvik, A., Bjørn, P., Ådlandsvik, B., Asplin, L., Skaròhamar, J., Johnsen, I., Myksvoll, M., Skogen, M., 2016. Toward a model-based prediction system for salmon lice infestation pressure. Aquacult. Environ. Interact. 8, 527–542. http://dx.doi.org/10.3354/aei00193.

Shchepetkin, A.F., McWilliams, J.C., 2005. The regional oceanic modeling system (ROMS): A split-explicit, free-surface, topography-following-coordinate oceanic model. Ocean Model. 9 (4), 347–404. http://dx.doi.org/10.1016/j.ocemod.2004.08.002.

Simonsen, K., Joensen, E., Erenbjerg, S., 2018. Sundalagiò - Samandráttur av hydrografiskum mátingum árini 2013-2017. In: Fiskaaling Rit. Technical Report, number 01, Fiskaaling P/F, Tórshavn, Faroe Islands, pp. 1–50.

Simpson, J.H., Sharples, J., 2012. Introduction to the Physical and Biological Oceanography of Shelf Seas. Cambridge University Press, http://dx.doi.org/10.1017/CBO9781139034098.

Skogseth, R., Asplin, L., Sandvik, A.D., 2007. Wind and tidal forcing on the mesoscale circulation in storfjorden, svalbard. Cont. Shelf Res. 27 (2), 208–227. http://dx.doi.org/10.1016/j.csr.2006.10.001.

Ullgren, J., Fer, I., Darelius, E., Beaird, N., 2014. Interaction of the faroe bank channel overflow with iceland basin intermediate waters. J. Geophys. Res.: Oceans 119 (1), 228–240. http://dx.doi.org/10.1002/2013JC009437.

Umlauf, L., Burchard, H., 2003. A generic length-scale equation for geophysical turbulence models. J. Mar. Res. 61, 235–265. http://dx.doi.org/10.1357/002224003322005087.